# A cautionary tale of topography and tilt from Kīlauea Caldera

**Jessica H. Johnson[1], Michael P. Poland[2], Kyle R. Anderson[3], and Juliet Biggs[4]**

[1]School of Environmental Sciences, University of East Anglia
[2]Cascades Volcano Observatory, US Geological Survey
[3]California Volcano Observatory, US Geological Survey
[4]School of Earth Sciences, University of Bristol

**Key Points:**

- Finite element analysis is used to investigate the effect of sharp topography on deformation
- Tilt magnitude and azimuth are drastically affected by the presence of a cliff
- Anomalous tilt at Kīlauea can be partially explained by the caldera topography



This article has been accepted for publication and undergone full peer review but has not been through the copyediting, typesetting, pagination and proofreading process which may lead to differences between this version and the Version of Record. Please cite this article as doi: 10.1029/2018GL081757

Corresponding author: Jessica Johnson, jessica.johnson@uea.ac.uk

**Abstract**

We conduct finite element analysis to investigate the effect of sharp topography on surface ground deformation caused by pressure changes in a magma reservoir. Tilt data expresses the horizontal gradient of vertical deformation and therefore can emphasise small variations in deformation that go unnoticed using other methods. We find that the vertical displacement profile at a surface with a cliff can be thought of as the superposition of the deformation from shallow and deeper sources. This combination can create a small peak in vertical displacement that acts as a pseudo-source, creating a reversal of the deformation gradient and therefore anomalous tilt magnitude and a rotation of up to 180°. We apply these models to Kīlauea Caldera and find that surface geometry creates a tilt rotation of $\sim 10°$, partially explaining anomalous tilt that has been observed. Our analysis highlights the importance of considering topography when assessing tilt measurements at active volcanoes.

## 1 Introduction

Surface deformation is often observed in connection with volcanic unrest. Common methods of monitoring volcano deformation include Global Navigation Satellite System (GNSS), synthetic aperture radar interferometry (InSAR) and tiltmeters (e.g. Dzurisin, 2006). Tiltmeters measure horizontal gradients (derivatives) of vertical displacements. As such, tilt can emphasise small variations in deformation that might go unnoticed in GNSS or InSAR data.

Observed volcano ground deformation has been attributed to a variety of mechanisms including magma intrusion (Dzurisin, 2003). Analytical solutions, such as the commonly used Mogi (1958) point-source model, can be used to predict deformation patterns. However, these analytical models assume a deep source in a homogeneous, elastic half-space – assumptions which are often violated in the real world (e.g. Cayol & Cornet, 1998). This analytical estimation breaks down under several conditions, including when the reservoir is shallow or the topography is steep. Models have been developed to overcome some of these assumptions, such as non-spherical source geometries (Yang, Davis, & Dieterich, 1988), subsurface heterogeneity (e.g. Masterlark, 2007), viscoelasticity (e.g. Del Negro, Currenti, & Scandura, 2009), and topographic corrections (Williams & Wadge, 1998, 2000). Williams and Wadge (1998) introduced a simple method of adjusting the elevation of the reference surface using analytical equations based on McTigue (1987) to account for topography. They later introduced a second method that can be used to account for topography by calculating higher-order corrections to approximate the slope (Williams & Wadge, 2000). However, the latter method is only effective when slopes are small.

The surface expressions of many volcanoes feature steep walls or cliffs. These cliffs are often part of calderas or caldera complexes but can also be caused by other processes such as rifting or sector collapse. Many calderas have steep bounding walls hundreds of meters high that plausibly could affect tilt measurements. Rhyolitic calderas can have $> 1$ km of subsidence of the caldera floor (Cole, Milner, & Spinks, 2005). The effect of sharp variations in topography such as cliffs has not been previously considered in studies of surface deformation in volcanic regions, even though they are a common feature. In addition, monitoring equipment is commonly placed on caldera rims as these locations are often more accessible (especially if the caldera is lake-filled) and have relatively less risk than more proximal locations, such as the caldera floor. Tilt measurements have played a significant role in the understanding of volcanic processes on at least 40 volcanoes worldwide (Gambino & Cammarata, 2017). Many volcanoes with tilt networks have steep topography. Cayol and Cornet (1998) constructed axis-symmetric models using finite element analysis (FEA) to investigate the effect of slopes up to 30° on tilt and found that in some cases, tilt at the summit of a volcano can be reversed relative to what would be expected with no topography. Neuberg, Collinson, Mothes, C. Ruiz, and Aguaiza (2018)

demonstrated that shear stress from magma ascending in a conduit can affect tilt measurements on the sloping ($< 30°$) flank of the cone at Tungurahua Volcano in Ecuador. Tilt records at several caldera volcanoes are difficult to explain with simple analytical models, including Campi Flegrei (Orsi, Petrazzuoli, & Wohletz, 1999), Miyakejima (Yamamoto, Ukawa, Fujita, Okada, & Kikuchi, 2001) and Rabaul (McKee et al., 1984). Here, we examine the effect of a step in topography on ground tilt caused by a simple inflation source and apply the model to Kīlauea Volcano in Hawai'i.

## 2 Models

To assess the control of sharp topography (i.e. a cliff) on surface deformation due to a pressurising magma reservoir, we constructed a 3D finite element model using COMSOL Multiphysics. We used three-dimensions to allow an azimuthal variation in tilt, which cannot be accounted for using axis-symmetric models (e.g. Cayol & Cornet, 1998; Hickey & Gottsmann, 2014). A simple model was constructed using the methods described in the Supplementary Material (S1) and parameters listed in Table S9, which were chosen to represent Kīlauea but are typical of basaltic shield volcanoes. Here we normalised distances by the depth of the pressure source ($z_{sphere}$) for ease of application to other systems. We used a fixed sphere radius ($r_{sphere}$) of 0.025 times $z_{sphere}$, and the height of the cliff ($C$) and the lateral distance of the cliff from the pressure source ($D$) were allowed to vary between 0.025 – 2 times $z_{sphere}$ and 0 –10 times $z_{sphere}$ respectively. We also normalised tilt and vertical displacement in our results because the outcomes scale with the ratio of the pressure of the source ($\Delta P$) to the shear modulus ($\mu$) (McTigue, 1987), and therefore are independent of the magnitude of deformation.

Vertical displacement and tilt vectors resulting from our Finite Element models can be seen in Figure 1. We observed that tilt, when measured just above the cliff, was different to that with no topography for all cliff geometries. This anomalous tilt is due to a small secondary peak in vertical displacement. This secondary peak is two orders of magnitude smaller than the peak deformation (Figure 1) and so is unlikely to be noticed in GNSS or InSAR measurements, but is visible in tilt measurements as tilt measures the gradient of displacement, rather than absolute ground displacement.

We suggest that the profile of vertical displacement in the presence of a cliff can be thought of as a combination of the displacement profiles from a deep source (depth $z_2 = z_{sphere}$) and a shallower source (depth $z_1 = z_{sphere} - C$, where $C$ is the height of the cliff) with no topography. This is because a shallow Mogi-type inflation source in a homogeneous elastic halfspace with no surface topography creates a profile of vertical deformation that has a relatively large maximum, and a relatively narrow peak (e.g. Figure 2, top, red). In contrast, when a source is deeper, the maximum vertical deformation is smaller and the curve is broader (e.g. Figure 2, top, blue). When the two vertical deformation profiles are plotted together, they will cross at a distance $r_c$ where:

$$r_c^2 = (1 - C)^{4/3} + (1 - C)^{2/3}. \quad (1)$$

In this equation, $r_c$ and $C$ are both normalised by $z_{sphere}$. Figure 2 (Top) displays the vertical displacement profiles for inflation sources at $z_1 = 0.95$ (red) and $z_2 = z_{sphere} = 1$ (blue) depth. The profile of vertical displacement in the presence of a cliff can be thought of as a superposition of both of these profiles (Figure 2 Top green, orange and magenta). In this case $z_1$ is the depth of the source beneath the caldera floor, and $z_2$ is the depth of the source beneath the top of the cliff, which is equal to $z_1 + C$, where $C = 0.05$ is the height of the cliff. Figure 2 (Middle) displays the radial tilt profiles for the same sources. Most of the tilt is positive because the ground is tilting away from the centre of inflation.

If the cliff is approximately the same distance away as the cross-over of the profiles ($D \sim r_c$), there will not be a sharp change in deformation gradient but rather a

smooth transition from one profile to the next (Figure 2 orange at $D = 1.38$). This can be seen in the transition from one tilt profile to the next without a significant change in magnitude. If the cliff is closer to the source than the cross-over of the profiles ($D < r_c$), there will be a sudden decrease in uplift with distance, seen in the tilt as a sharp peak, but the gradient will not change sign and so the tilt will stay positive (Figure 2 magneta). However, this necessarily means that if the cliff is farther away from the source than the cross-over of the profiles ($D > r_c$), there will be a local secondary maximum in the vertical displacement, and hence an inversion of the deformation gradient (Figure 2 green). In our example, when the cliff is 2 times $z_{sphere}$ away from the centre (green), the inversion of the deformation gradient can be seen where the tilt becomes negative, which means that the ground is tilting towards the inflation source.

The effect of the cliff in the tilt can be seen in both the finite element analysis (Figure 2, left), and the analytical solutions (Figure 2, right) using a method similar to Williams and Wadge (1998). However, using FEA, each element communicates with its neighbours, resulting in the reversal of tilt being smoothed across a wider distance compared to the analytical models, where each point is calculated individually.

Equation 1 can be used to predict the existence of the secondary lobe, but does not contain information about the magnitude of the lobe, nor where the peak is relative to the cliff. The magnitude of the secondary maximum or lobe is dependent on the difference between the cliff-free deformation using source depths of $z_1$ and $z_2$. This is a function of the difference in depths ($z_2 - z1 = C$, height of the cliff) and the horizontal distance of the cliff from the source ($D$). Figure 3 (blue) shows the maximum vertical displacement in the secondary lobe for $C = 0.025$, 0.5 and 1.5 times $z_{sphere}$, for $D = 0-5$ times $z_{sphere}$. This secondary lobe of deformation will have a maximum magnitude if the cliff is located where the difference between the profiles is the greatest while $D > r_c$.

The distance of the lobe from the cliff is also dependent on $C$ and $D$. Figure 3 (red) shows the distance of the lobe from the cliff for $C = 0.025$, 0.5 and 1.5 times $z_{sphere}$, and $D = 0 - 5$ times $z_{sphere}$. As $D$ increases, the distance of the lobe from the cliff increases.

Figure 1 displays oblique views of the 3D FEA models for a 1 MPa inflation source with a normalised cliff height of 0.25. Coloured contours show the small interval of vertical displacement in which the secondary lobes are visible, and black arrows show tilt azimuth and magnitude. When a linear cliff is used, the secondary lobe creates an elongated virtual deformation source on the cliff (Figure 1 a, b). This virtual source causes tilt vectors to be rotated from their expected azimuth. When $D > r_c$ (Figure 1 a), the secondary lobe of deformation causes nearby tilt vectors to rotate away from it. When $D < r_c$ (Figure 1 b), the gradient of deformation is not reversed but there is a steepening in an elongated area. This causes the tilt vectors to have a greater magnitude further away from the cliff, and to rotate toward the expected deformation pattern from the primary source.

An axi-symmetric model allows the effect of the secondary lobe on a circular caldera to be viewed (Figure 1 c). In this case the lobe is circular and therefore does not affect the azimuth of the tilt vectors except for the space between the cliff edge and the lobe maximum. In this region, the tilt vector will be rotated by 180°. Further away from the cliff edge, vector azimuths can be well approximated by a half-space analytical solution. The tilt magnitude is also affected by the presence of the secondary lobe, with it tending to zero close to the peak of the lobe. Above the cliff, tilt magnitude will be slightly larger than expected but the two profiles become more similar as they tend toward zero deformation.

## 3 Case Study: Kīlauea Volcano

Kīlauea Volcano is a basaltic shield volcano on the Island of Hawai'i (Figure 4). Between 1983 and 2018, eruptive activity was fairly stable with occasional minor shifts (Orr et al., 2015). During that time period there were two primary eruptive centres; along the East Rift Zone centred on the vicinity of the Pu'u 'Ō'ō cone starting in 1983, and at the summit from a lava lake contained within a vent along the southeast side of Halema'uma'u crater starting in 2008. Both of these vents ceased activity in mid-2018 due to a major Lower East Rift Zone lava effusion and summit collapse.

Evidence for the geometry of the magmatic plumbing system at Kīlauea comes largely from deformation data (Poland, Miklius, & Montgomery-Brown, 2014). The so-called Halema'uma'u (HMM) deformation source is the shallowest magma reservoir at approximately 1 km below the surface, centred just to the east of Halema'uma'u crater (Figure 4). Large-scale deformation during eruption and intrusion events has been attributed to this hypothesised reservoir (e.g. Lundgren et al., 2013). Several authors have estimated the depth of the HMM reservoir using geodetic, seismic and petrological evidence, and depths range from 0.2 to 5 km below the surface, with the majority of estimates around 1 km below the floor of Kīlauea Caldera (e.g. Almendros, Chouet, Dawson, & Bond, 2002; Battaglia, Got, & Okubo, 2003; Cervelli & Miklius, 2003; Chouet, Dawson, James, & Lane, 2010; Dawson et al., 1999; Dzurisin et al., 1980; Johnson et al., 2010; Ohminato, Chouet, Dawson, & Kedar, 1998; Poland et al., 2014; Ryan, 1988; Thornber, Orr, Heliker, & Hoblitt, 2015).

Transient deformation events with shorter durations and smaller magnitudes have also been observed as originating from the HMM source. These so-called deflation-inflation (DI) events have been detected with GNSS and InSAR, but have been particularly well recorded by the network of borehole electronic tiltmeters since 1999. The deformation source appears constant over time (Anderson et al., 2015). These repeating events have the benefit that the data can be stacked to increase the signal-to-noise ratio, and can be used to accurately locate the HMM source. Anderson et al. (2015) used a bayesian inverse formulation with a Markov Chain Monte Carlo algorithm to locate the source of DI events to within 600 m horizontally. Several factors including the geometry of the tilt network, however, prevented the accurate estimation of the depth of this source. Anderson et al. (2015) also noted that, although inversions using most of the summit tiltmeters yielded low errors, one tiltmeter (SMC, Figure 4) consistently degraded the result of the inversions. This was because the vectors from the DI events were consistently rotated by about 25° anti-clockwise from that predicted by analytical models (Figure 4). Anderson et al. (2015) proposed several possible reasons for the consistent misfit of SMC, including the effect of local topography.

Tiltmeter SMC is located near a section of the caldera rim that is more linear than other parts of the caldera (Figure 4). The difference of the azimuth and magnitude of tilt at tiltmeter SMC relative to that predicted from a simple analytical model (Figure 4) has been calculated as 28±2° and 20±5% respectively (Anderson et al., 2015). Therefore, to model the effect of the linear portion of the caldera rim and investigate whether the difference in tilt data can be explained by topography, the top boundary was approximated with a single linear vertical cliff. We conducted a grid search over the depth of the pressure source to find a model that best fits the data. For these models, we no longer normalise the distances.

If we assume that the horizontal location of the HMM source is well constrained (Anderson et al., 2015), we can rotate the reference frame so that the centre of the deformation source is at $x = 0, y = 0$, the top of the cliff is at $z = 0$, and the cliff in the vicinity of SMC runs parallel to the y-axis. The cliff is known to be 80 m high ($C = 80$m) and tiltmeter SMC is approximately 200 m from the cliff edge ($x_{tilt} = 200$m). The dis-

tance between the HMM reservoir and the cliff ($D$) is approximately 1000 m and tiltmeter SMC is approximately 1500 m along the cliff ($y_{tilt} = 1500$m).

Using these values, the depth at which the crossover distance ($r_c$) equals $D$ is $z_2 =$ 748 m from the caldera floor, using equation 1. Therefore, the maximum $z_1$ is 750 m. We assign the minimum $z_1$ as 500 m (the *a priori* limit set by previous observations, see Anderson et al. (2015) for details). Using $D$, $C$, $x_{tilt}$ and $y_{tilt}$ defined above and $z_1 =$ 500 m, a secondary lobe is created with its peak only 40.9 m away from the cliff edge. The tiltmeter is far enough away from the secondary lobe that the effect of the secondary lobe is much less than if the tiltmeter were closer, with a tilt rotation of only 10° and a change in tilt magnitude of only 20%. With $z_2 = 750$ m, the deformation of the lobe is not greater than the deformation at the cliff edge, and the tilt at SMC is affected even less than with a shallower source. We found that changing the radius of the source did not significantly affect these results (see Supplementary Material S6 for more information).

The same analysis for tiltmeter UWE, using $D = 1500$ m, $C = 85$ m, $x_{tilt} =$ 660 m and $y_{tilt} = 0$, does not rotate the tilt vector as the cliff is perpendicular to the source-tiltmeter line. However, the magnitude of the tilt at UWE is 6% larger, indicating that inversions for the pressure source using this tiltmeter could also be influenced by the topography. There is not a significant cliff between SDH and the source (17 m), so this analysis would not elucidate any discrepancies in the data from SDH. Tiltmeter IKI is about 500 m away from the edge of Kīlauea caldera and so the topography of that caldera does not have a significant effect on the tilt here when the deformation is caused by the HMM source. However, IKI is also near to the edge of Kīlauea Iki crater, which is over 100 m deep in places. If there was a deformation source related to Kīlauea Iki crater, then it is likely that the more complex topography around IKI would influence the tilt there. Models with realistic topography (Supplementary Material S7) also indicate that the rotation at these other tiltmeters is negligible.

Despite the models of idealised topography displaying tilt rotations of up to 180°, the geometry at Kīlauea only allows a maximum rotation of tilt at SMC of 10°. Models using the same source geometry with realistic topography (Supplementary Material S9) agree with this rotation. Therefore, the anomalous tilt data at Kīlauea cannot be completely explained by the presence of a topographic step, although we have shown that it exerts significant influence. The simple model with homogeneous physical properties and a spherical pressure source is not adequate to fully explain the anomalous tilt data. We suggest that a more complex source geometry, as suggested by the shape of the partial caldera collapse during the 2018 Lower East Rift Zone eruption, and material heterogeneity, are likely to contribute to the rotation of the tilt data.

The 2018 collapse at Kīlauea summit has reshaped the cliffs around the caldera (Wasser & Benitez, 2018). The new geometry has near-vertical cliffs of up to 500 m and terrace-like steps of 50-150 m. These new structures may have an impact on tilt measured at the existing network of tiltmeters and have implications for any new monitoring equipment that is installed.

## 4 Conclusions

We have conducted finite element analysis of deformation due to a shallow pressure source to characterise the effect of sharp changes in topography. Our results show that steps in topography such as caldera rims can create a secondary lobe of deformation, which can affect tilt data. We have devised a simple relationship between geometry elements (the depth of the pressure source, the height of the cliff, and the distance of the cliff from the pressure source) that allows us to predict the existence of the secondary lobe. Where a secondary lobe is created, its size is as much as two orders of mag-

nitude smaller than the main deformation and so is unlikely to be noticed in GNSS or InSAR measurements, but will be visible in tilt measurements, as tilt measures the gradient of displacement, rather than absolute ground displacement. Our models show that when a cliff runs perpendicular to a line between the source and a tiltmeter then only the tilt magnitude is affected. However, if the cliff is oblique then the tilt azimuth can be rotated by up to 180°, which may introduce errors in data inversion.

During 1999-2018, borehole tilt data at Kīlauea Volcano were often characterised by small deformation events that were highly repeatable. These repeating deformation events allow the magma reservoir, in which the pressure transients were occurring, to be well characterised except for the depth of the reservoir. One tiltmeter, located near a linear section of the caldera rim, persistently displayed deformation that does not fit with other data. Our finite element models were applied to a simplified Kīlauea summit caldera to investigate whether the anomalous data from this tiltmeter could be due to topography. We found that the geometry of Kīlauea Caldera up to early 2018 meant that the maximum tilt rotation from topographic effects was 10°, compared to an observed discrepancy of about 25° between the anomalous tiltmeter data and analytical models that best fit data from other tiltmeters. Therefore, the anomalous tilt data at Kīlauea cannot be completely explained by topography, although that may exert some influence. Nevertheless, our analysis does point to the importance of considering topography when assessing tilt measurements at active volcanoes.

These findings have implications for network design and show that sharp topography can have dramatic effects on tilt data. This also implies that other tiltmeters around Kīlauea and other volcanoes globally could be affected by caldera rims and other sharp topography, and so tilt magnitude and azimuth should be treated with caution.

**Acknowledgments**

We would like to thank a USGS-UHH cooperative agreement and Marie Curie ( FP7-MC-IIF 328870) for funding this work. COMSOL models are available in the supporting material. We would also like to thank Freysteinn Sigmundsson, Maurizio Battaglia, Daniel Dzurisin and an anonymous reviewer for their detailed and insightful comments.

## References

Almendros, J., Chouet, B., Dawson, P., & Bond, T. (2002, feb). Identifying elements of the plumbing system beneath Kilauea Volcano, Hawaii, from the source locations of very-long-period signals. *Geophysical Journal International*, *148*(2), 303–312. Retrieved from `http://gji.oxfordjournals.org/cgi/doi/10.1046/j.1365-246X.2002.01629.x` doi: 10.1046/j.1365-246X.2002.01629.x

Anderson, K. R., Poland, M. P., Johnson, J. H., & Miklius, A. (2015). *Episodic Deflation–Inflation Events at Kılauea Volcano and Implications for the Shallow Magma System Kyle* (First ed., Vol. 208; R. Carey, V. Cayol, M. Poland, & D. Weis, Eds.). Hoboken, NJ: John Wiley & Sons, Inc. Retrieved from `http://doi.wiley.com/10.1002/9781118872079` doi: 10.1002/9781118872079

Battaglia, J., Got, J. L., & Okubo, P. (2003). Location of long-period events below Kilauea Volcano using seismic amplitudes and accurate relative relocation. *Journal of Geophysical Research*, *108*(B12), 2553. Retrieved from `http://www.agu.org/pubs/crossref/2003/2003JB002517.shtmlhttp://www.agu.org/pubs/crossref/2003/2002JB002193.shtmlhttp://doi.wiley.com/10.1029/2003JB002517` doi: 10.1029/2003JB002517

Cayol, V., & Cornet, F. H. (1998, jun). Effects of topography on the interpretation of the deformation field of prominent volcanoes: Application to Etna. *Geophysical Research Letters*, *25*(11), 1979–1982. Retrieved from `http://doi.wiley`

.com/10.1029/98GL51512 doi: 10.1029/98GL51512

Cervelli, P. F., & Miklius, A. (2003). The Shallow Magmatic System of Kilauea Volcano. In C. Heliker, D. A. Swanson, & T. J. Takahashi (Eds.), *The pu'u 'Ō'ō–kūpaianahā eruption of kīlauea volcano, hawai'i: the first 20 years* (pp. 149–164). Reston, Virginia: U.S Geological Survey Professional Paper 1676. Retrieved from http://books.google.com/books?hl=en{\&}lr={\&}id=9B{_}wAAAAMAAJ{\&}oi=fnd{\&}pg=PA149{\&}dq=The+shallow+magmatic+system+of+Kilauea+volcano{\&}ots=7Cx98meobj{\&}sig=zkSeHLkVrwv88Q4qMH7frCTIxNU

Chouet, B. A., Dawson, P. B., James, M. R., & Lane, S. J. (2010, sep). Seismic source mechanism of degassing bursts at Kilauea Volcano, Hawaii: Results from waveform inversion in the 10–50 s band. *Journal of Geophysical Research*, *115*(B9), B09311. Retrieved from http://doi.wiley.com/10.1029/2009JB006661 doi: 10.1029/2009JB006661

Cole, J., Milner, D., & Spinks, K. (2005, feb). Calderas and caldera structures: a review. *Earth-Science Reviews*, *69*(1-2), 1–26. Retrieved from http://linkinghub.elsevier.com/retrieve/pii/S0012825204000868 doi: 10.1016/j.earscirev.2004.06.004

Dawson, P. B., Chouet, B. A., Okubo, P. G., Villaseñor, A., Benz, H. M., & Villasenor, A. (1999, sep). Three-dimensional velocity structure of the Kilauea caldera, Hawaii. *Geophysical Research Letters*, *26*(18), 2805–2808. Retrieved from http://www.agu.org/pubs/crossref/1999/1999GL005379.shtmlhttp://doi.wiley.com/10.1029/1999GL005379 doi: 10.1029/1999GL005379

Del Negro, C., Currenti, G., & Scandura, D. (2009, feb). Temperature-dependent viscoelastic modeling of ground deformation: Application to Etna volcano during the 1993–1997 inflation period. *Physics of the Earth and Planetary Interiors*, *172*(3-4), 299–309. Retrieved from http://linkinghub.elsevier.com/retrieve/pii/S0031920108003087 doi: 10.1016/j.pepi.2008.10.019

Dzurisin, D. (2003). A comprehensive approach to monitoring volcano deformation as a window on the eruption cycle. *Reviews of Geophysics*, *41*(1), 1001. Retrieved from http://www.agu.org/pubs/crossref/2003/2001RG000107.shtmlhttp://doi.wiley.com/10.1029/2001RG000107 doi: 10.1029/2001RG000107

Dzurisin, D. (2006). *Volcano Deformation*. Berlin, Heidelberg: Springer Berlin Heidelberg. Retrieved from http://link.springer.com/10.1007/978-3-540-49302-0 doi: 10.1007/978-3-540-49302-0

Dzurisin, D., Anderson, L. A., Eaton, G. P., Koyanagi, R. Y., Lipman, P. W., Lockwood, J. P., ... Yamashita, K. M. (1980, may). Geophysical observations of Kilauea Volcano, Hawaii, 2. Constraints on the magma supply during November 1975- September 1977. *Journal of Volcanology and Geothermal Research*, *7*(3-4), 241–269. Retrieved from http://linkinghub.elsevier.com/retrieve/pii/0377027380900323 doi: 10.1016/0377-0273(80)90032-3

Gambino, S., & Cammarata, L. (2017, jun). Tilt measurements on volcanoes: more than a hundred years of recordings. *Italian Journal of Geosciences*, *136*(2), 275–295. Retrieved from http://www.italianjournalofgeosciences.it/244/fulltext.html?ida=734 doi: 10.3301/IJG.2017.07

Hickey, J., & Gottsmann, J. (2014, may). Benchmarking and developing numerical Finite Element models of volcanic deformation. *Journal of Volcanology and Geothermal Research*, *280*, 126–130. Retrieved from http://linkinghub.elsevier.com/retrieve/pii/S037702731400153X doi: 10.1016/j.jvolgeores.2014.05.011

Johnson, D. J., Eggers, A. A., Bagnardi, M., Battaglia, M., Poland, M. P., & Miklius, A. (2010, nov). Shallow magma accumulation at Kilauea Volcano, Hawai'i, revealed by microgravity surveys. *Geology*, *38*(12), 1139–1142. Re-

trieved from http://geology.gsapubs.org/cgi/doi/10.1130/G31323.1 doi: 10.1130/G31323.1

Lundgren, P., Poland, M., Miklius, A., Orr, T., Yun, S.-H., Fielding, E., ... Owen, S. (2013, mar). Evolution of dike opening during the March 2011 Kamoamoa fissure eruption, Kīlauea Volcano, Hawai'i. *Journal of Geophysical Research: Solid Earth*, *118*(3), 897–914. Retrieved from http://doi.wiley.com/10.1002/jgrb.50108 doi: 10.1002/jgrb.50108

Masterlark, T. (2007, jun). Magma intrusion and deformation predictions: Sensitivities to the Mogi assumptions. *Journal of Geophysical Research*, *112*(B6), B06419. Retrieved from http://www.agu.org/pubs/crossref/2007/2006JB004860.shtml doi: 10.1029/2006JB004860

McKee, C. O., Lowenstein, P. L., De Saint Ours, P., Talai, B., Itikarai, I., & Mori, J. J. (1984). Seismic and ground deformation crises at Rabaul Caldera: Prelude to an eruption? *Bulletin Volcanologique*, *47*(2), 397–411. doi: 10.1007/BF01961569

McTigue, D. F. (1987). Elastic stress and deformation near a finite spherical magma body: Resolution of the point source paradox. *Journal of Geophysical Research*, *92*(B12), 12931. Retrieved from http://doi.wiley.com/10.1029/JB092iB12p12931 doi: 10.1029/JB092iB12p12931

Mogi, K. (1958). Relations between the eruptions of various volcanoes and the deformations of the ground surfaces around them. *Bulletin of the Earthquake Research Institute*, *Vol. 36*, 99–134.

Neuberg, J. W., Collinson, A. S., Mothes, P. A., C. Ruiz, M., & Aguaiza, S. (2018). Understanding cyclic seismicity and ground deformation patterns at volcanoes: Intriguing lessons from Tungurahua volcano, Ecuador. *Earth and Planetary Science Letters*, *482*. doi: 10.1016/j.epsl.2017.10.050

Ohminato, T., Chouet, B. A., Dawson, P. B., & Kedar, S. (1998). Waveform inversion of very long period impulsive signals associated with magmatic injection beneath Kilauea volcano, Hawaii. *Journal of Geophysical Research*, *103*(B10), 23839. Retrieved from http://www.agu.org/pubs/crossref/1998/98JB01122.shtml doi: 10.1029/98JB01122

Orr, T. R., Poland, M. P., Patrick, M. R., Thelen, W. A., Sutton, A. J., Elias, T., ... Wooten, K. M. (2015, feb). Kīlauea's 5-9 March 2011 Kamoamoa Fissure Eruption and Its Relation to 30+ Years of Activity From Pu'u 'Ō 'ō. In R. Carey, V. Cayol, M. Poland, & D. Weis (Eds.), *Hawaiian volcanoes: From source to surface, geophysical monograph, american geophysical union* (Vol. 208, pp. 393–420). Hoboken, NJ: John Wiley & Sons, Inc. Retrieved from http://doi.wiley.com/10.1002/9781118872079.ch18 doi: 10.1002/9781118872079.ch18

Orsi, G., Petrazzuoli, S. M., & Wohletz, K. (1999). Mechanical and thermofluid behaviour during unrest at the Campi Flegrei caldera (Italy). *Journal of Volcanology and Geothermal Research*, *91*(2-4), 453–470. doi: 10.1016/S0377-0273(99)00051-7

Poland, M. P., Miklius, A., & Montgomery-Brown, E. K. (2014). Magma supply, storage, and transport at shield-stage Hawaiian volcanoes. In *Characteristics of hawaiian volcanoes* (chap. 5). USGS. doi: 10.3133/pp18015

Ryan, M. P. (1988). The mechanics and three-dimensional internal structure of active magmatic systems: Kilauea Volcano, Hawaii. *Journal of Geophysical Research*, *93*(B5), 4213. Retrieved from http://doi.wiley.com/10.1029/JB093iB05p04213 doi: 10.1029/JB093iB05p04213

Thornber, C. R., Orr, T. R., Heliker, C., & Hoblitt, R. P. (2015, feb). Petrologic Testament to Changes in Shallow Magma Storage and Transport During 30+ Years of Recharge and Eruption at Kīlauea Volcano, Hawai'i. In R. Carey, V. Cayol, M. Poland, & D. Weis (Eds.), *Hawaiian volcanoes: From source to surface, geophysical monograph, american geophysical union*

(Vol. 208, pp. 147–188). Hoboken, NJ: John Wiley & Sons, Inc. Retrieved from http://doi.wiley.com/10.1002/9781118872079.ch8 doi: 10.1002/9781118872079.ch8

Wasser, M., & Benitez, D. (2018). *2018 HAVO increased Volcanic Activity Kīlauea Summit Fault Lines Map* (Tech. Rep.). NPS GISS.

Williams, C. A., & Wadge, G. (1998, may). The effects of topography on magma chamber deformation models: Application to Mt. Etna and radar interferometry. *Geophysical Research Letters*, *25*(10), 1549–1552. Retrieved from http://doi.wiley.com/10.1029/98GL01136 doi: 10.1029/98GL01136

Williams, C. A., & Wadge, G. (2000). An accurate and efficient method for including the effects of topography in three-dimensional elastic models of ground deformation with applications to radar interferometry. *Journal of Geophysical Research*, *105*(B4), 8103–8120. doi: 10.1029/1999JB900307

Yamamoto, E., Ukawa, M., Fujita, E., Okada, Y., & Kikuchi, M. (2001). Step-like Tilt Change Occurred during the Caldera-forming Stage of the 2000 Miyakejima Volcanic Activity. *Journal of Geography*, *110*(2), 181–190.

Yang, X.-M., Davis, P. M., & Dieterich, J. H. (1988). Deformation From Inflation of a Dipping Finite Prolate Spheroid in an Elastic Half-Space as a Model for Volcanic Stressing. *Journal of Geophysical Research*, *93*(B5), 4249–4257. doi: 10.1029/JB093iB05p04249

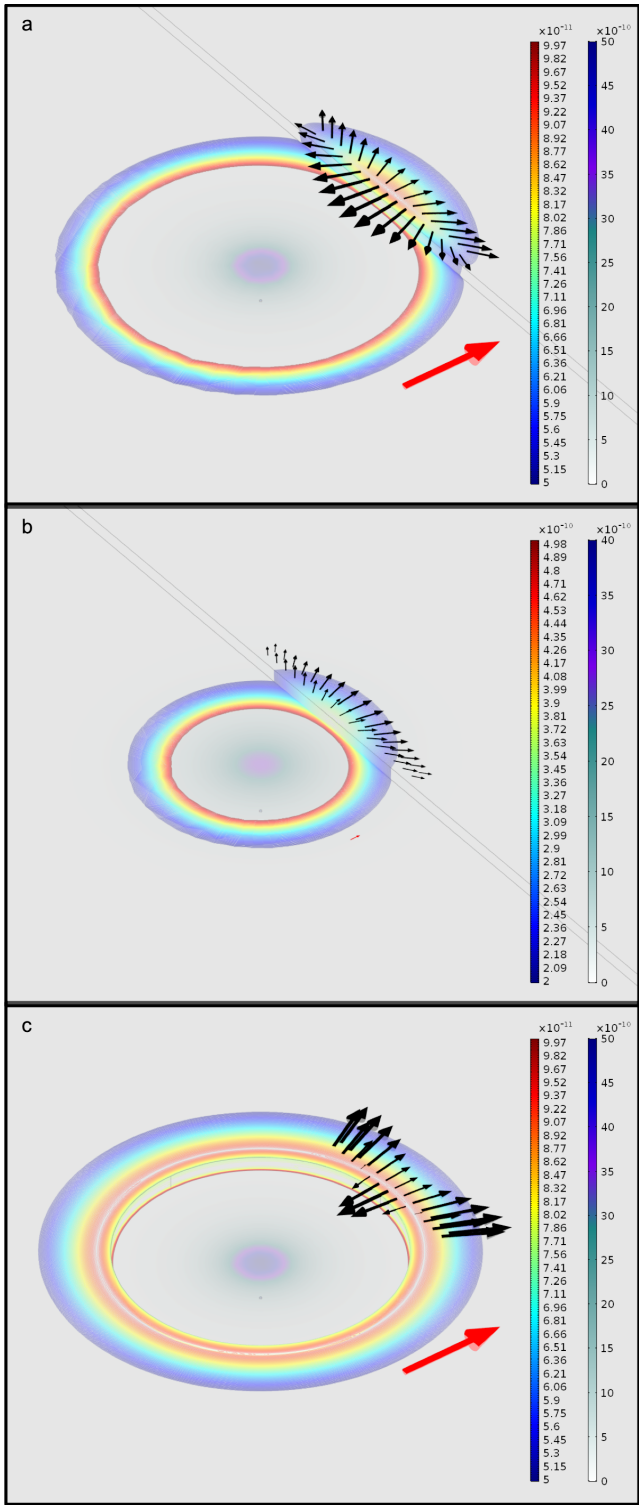


**Figure 1.** Deformation using parameter values from Table S9. Black arrows show tilt vectors, with red arrow indicating $0.1\mu rad$. Colours show normalised vertical displacement with cold colours showing full deformation field and bright coloured contours showing a narrow range around the lobe displacement. a) Deformation above a linear cliff with normalised height of 0.25, at a normalised distance of 2.5 horizontally away from the source. b) Deformation above a linear cliff with normalised height of 0.25, at a normalised distance of 1.25 horizontally away from the source. c) Deformation above a circular (caldera-like) cliff with normalised height of 0.25, at a normalised distance of 2.5 horizontally away from the source.

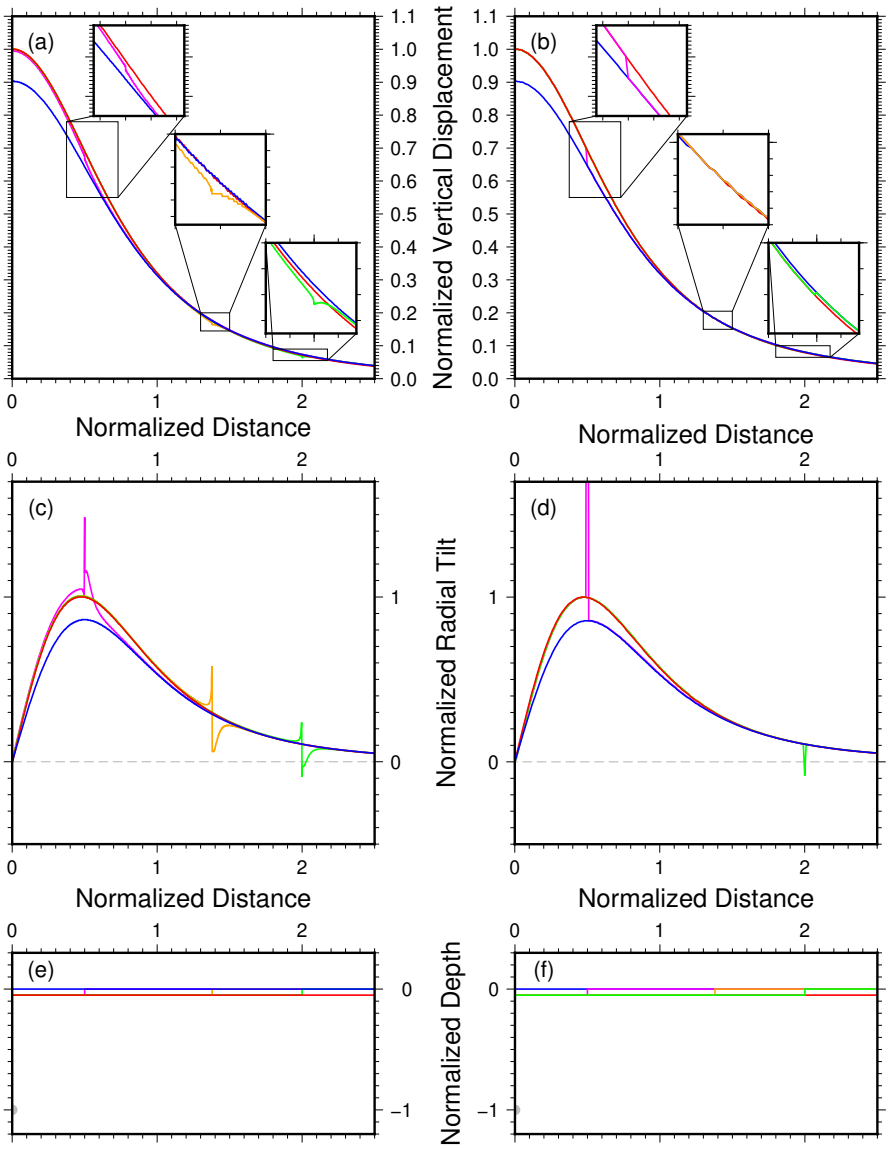


**Figure 2.** Deformation profiles for spherical inflation sources using parameter values from Table S9. Left panels (a and c) show results from FEA. Right show results from an analytical model similar to Williams and Wadge (1998). Top panels (a and b) show the vertical displacement profiles at the surface, normalized by the sphere depth. Middle panels (c and d) show the normalized radial tilt profile. Bottom panels (e and f) show schematics of the models with grey circles representing the inflating pressure source. (e) and (f) are the same but are plotted with different topographies illustrated. In all plots red shows the profiles with the source $0.95 \times z_{sphere}$ below a flat surface, blue shows the profiles with the source $1 \times z_{sphere}$ below a flat surface. Green, orange and magenta show the profiles for a source depth of $1 \times z_{sphere}$ with a cliff located at 0.5, 1.38 and $2 \times z_{sphere}$ away respectively.

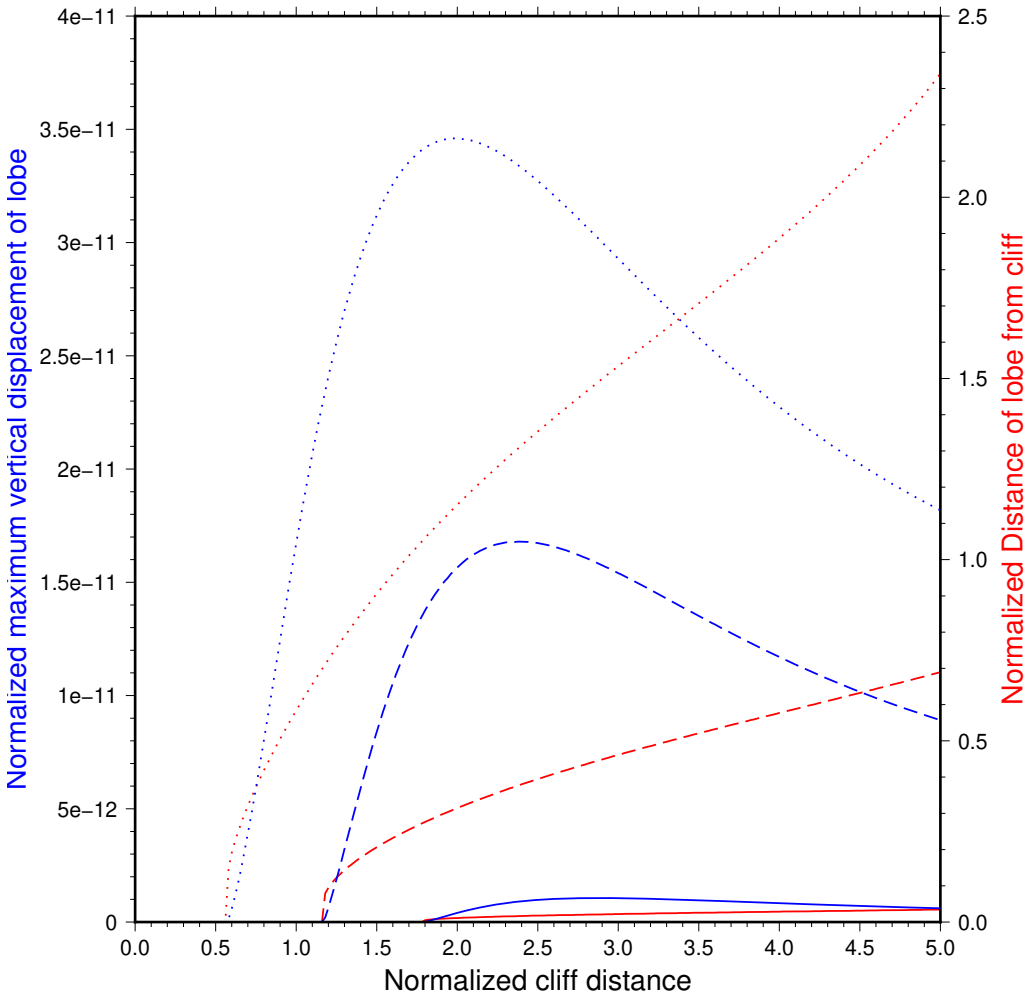


**Figure 3.** Magnitude and location of the secondary lobe of vertical displacement from a spherical inflation source using parameter values from Table S9 . Blue shows the maximum magnitude of the vertical deformation of the secondary lobe compared to the deformation at the cliff edge. Red shows the distance of the peak of the secondary lobe from the cliff edge. Solid line is for $C = 0.025$, dashed line is for $C = 0.5$, and dotted line is for $C = 1.5$ times $z_{sphere}$.

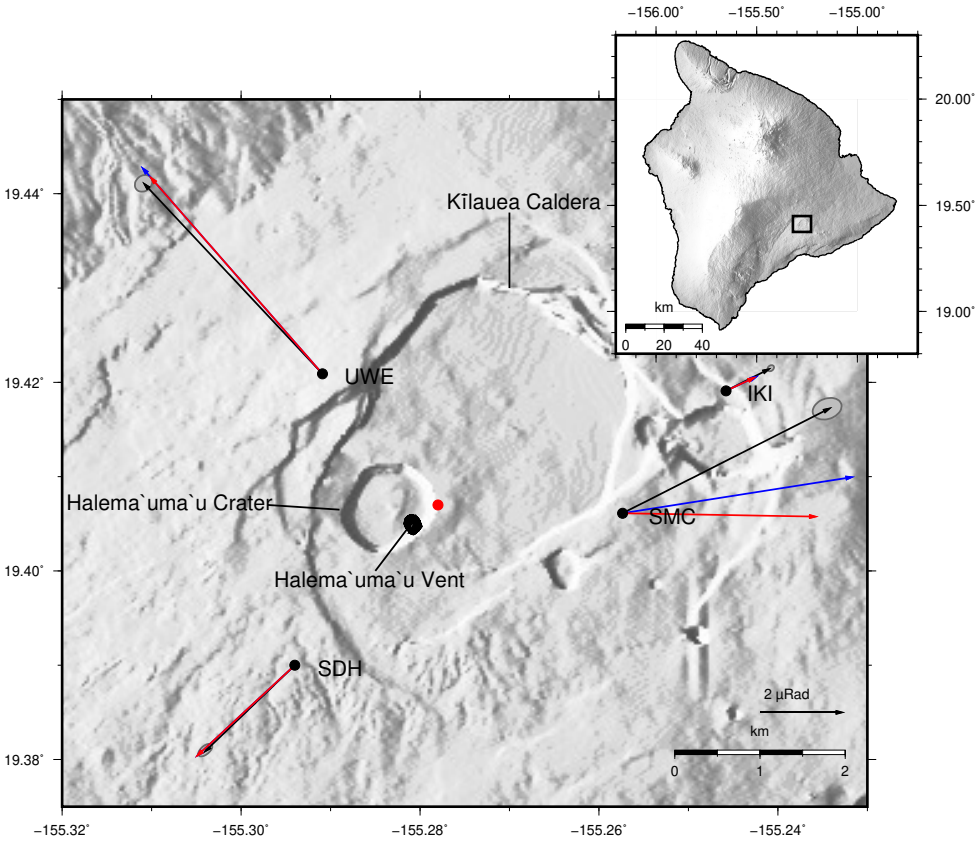


**Figure 4.** Map of Kīlauea Caldera showing tiltmeters (black circles) and hypothesised Halema‘uma‘u reservoir as red circle. Black vectors indicate averaged tilt data for DID-type events with 95% error ellipses. Red vectors indicate modelled tilt from best fitting Mogi-type inflation source (red circle) from Anderson et al. (2015). Blue vector indicates modelled tilt vectors with simple cliff topography. Inset shows study area location on the Island of Hawai‘i.

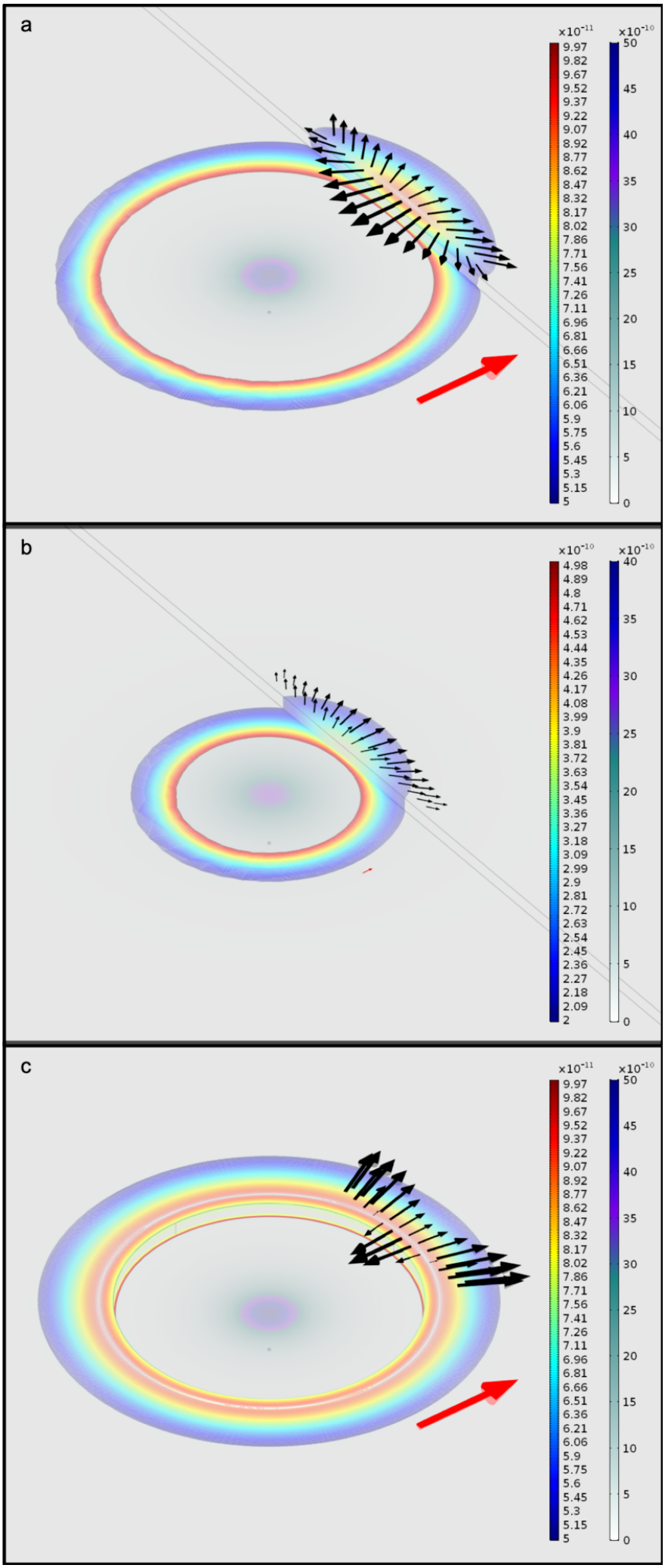


2018GL081757-f01-z-.png

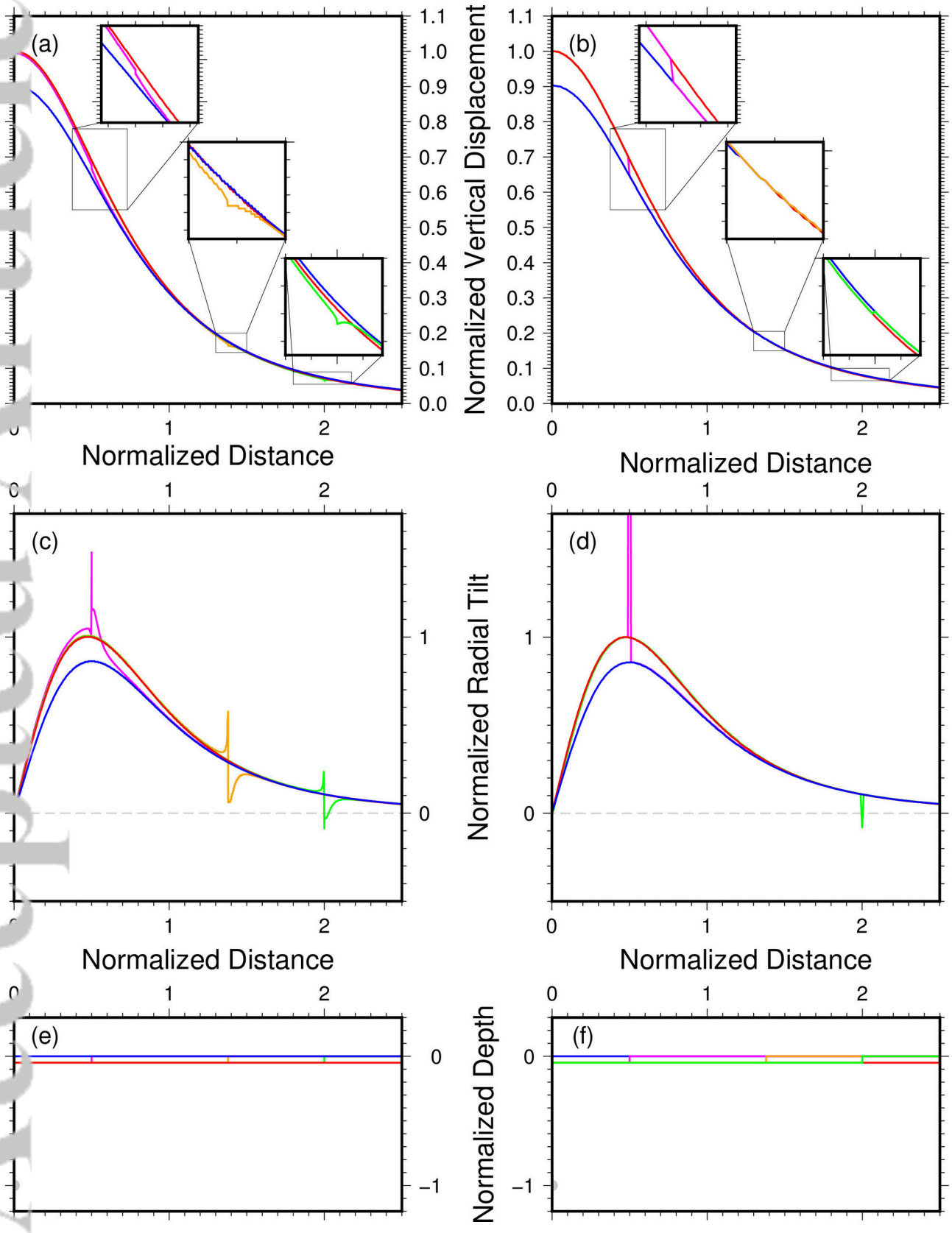


2018gl081757-f02-z-.eps

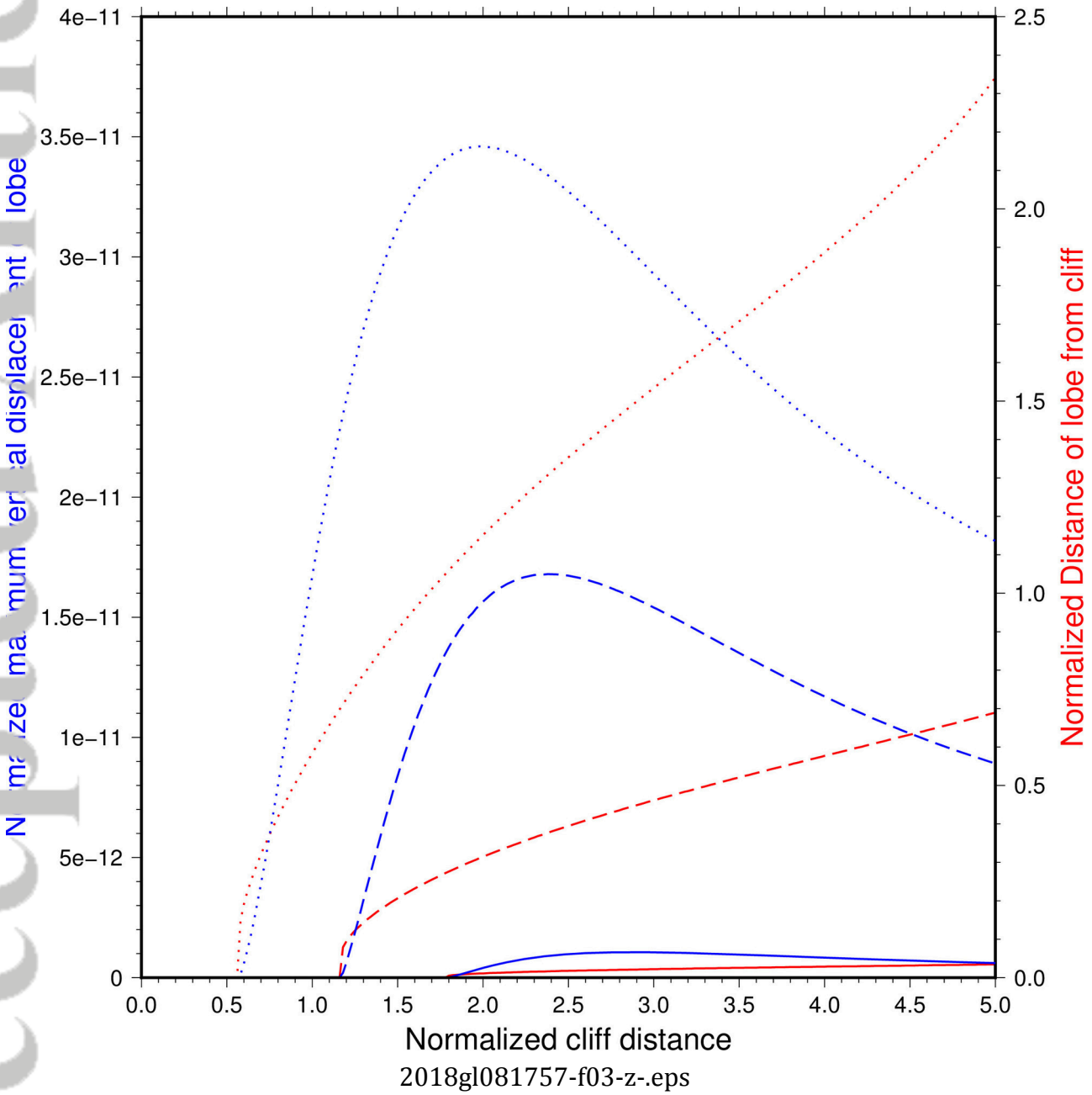

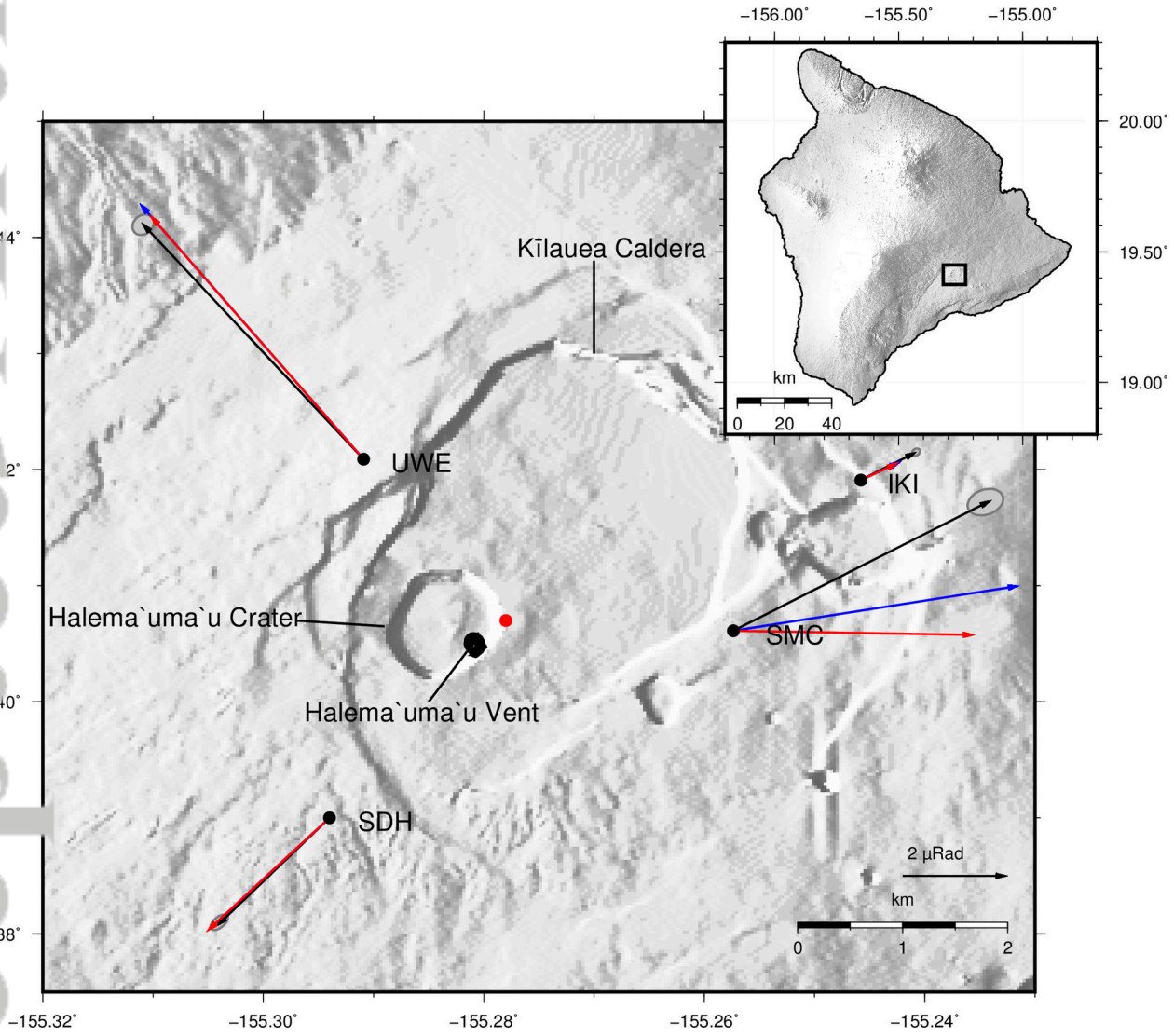


2018gl081757-f04-z-.eps